Surface-Plasmon Resonance-Enhanced Multiphoton Emission of High-Brightness Electron Beams from a Nanostructured Copper Cathode

R. K. Li, H. To, G. Andonian, J. Feng, A. Polyakov, C. M. Scoby, K. Thompson, W. Wan, H. A. Padmore, and P. Musumeci

Phys. Rev. Lett. **110**, 074801 — Published 11 February 2013

DOI: 10.1103/PhysRevLett.110.074801

Surface Plasmon Resonance Enhanced Multiphoton Emission of High Brightness Electron Beams from a Nanostructured Copper Cathode

R. K. Li,[1] H. To,[1] G. Andonian,[1] J. Feng,[2] A. Polyakov,[2] C. M. Scoby,[1] K. Thompson,[2] W. Wan,[2] H. A. Padmore,[2] and P. Musumeci[1,*]

[1] *Department of Physics and Astronomy, UCLA, Los Angeles, California 90095, USA*
[2] *Advanced Light Source Division, LBNL, Berkeley, California 94720, USA*

We experimentally investigate surface plasmon assisted photoemission to enhance the efficiency of metallic photocathodes for high brightness electron sources. A nanohole array-based copper surface was designed to exhibit a plasmonic response at 800 nm, fabricated using focused ion beam milling technique, optically characterized and tested as a photocathode in a high power radiofrequency photoinjector. Due to larger absorption and localization of the optical field intensity, the charge yield observed under ultrashort laser pulse illumination is increased by more than one hundred times compared to a flat surface. We also present the first beam characterization results (intrinsic emittance and bunch length) from a nanostructured photocathode.

PACS numbers: 29.25.Bx, 41.75.Ht, 79.60.-i, 78.67.-n

Recent progress in nanotechnologies has enabled fine control of the optical properties of metal surfaces by shaping them with sub-optical-wavelength features [1]. At nanostructured interfaces strong coupling can occur between light and the metal electron oscillations or surface plasmons (SPs). By tailoring the SP properties, controlled by the physical dimensions of the nanostructures, one can greatly enhance light absorption, transmission or reflection at selected wavelengths, and localize the optical field intensity. This phenomena has sparked great research interests related to laser-material interactions on nanometer-femtosecond scales and many entailing exotic applications in, for example, optics, magneto-optic data storage, and sub-wavelength detection of biomolecules [2–4].

An interesting open question deals with the possibility to exploit these plasmonic effects to manipulate not only the optical, but also the photoemission response. This could open novel possibilities in the field of the generation of picosecond to femtosecond high brightness electron beams, which are the enabling technology for many revolutionary scientific tools [5]. Due to their prompt response, low vacuum requirements and robustness, metals (in many cases simple copper) are usually the preferred choice in high peak brightness photoguns. However, in high repetition rate and high average current beams applications, metals are less viable because they typically require ultraviolet (UV) laser pulses and are characterized by low intrinsic quantum efficiency (QE), hence requiring exceedingly high average power of drive laser. To this end, there are extensive research efforts on semiconductor cathodes [6] which have 2-3 orders of magnitude higher QE and can reach up to GHz repetition rate. Semiconductor cathodes also feature more complicated fabrication procedures, more stringent vacuum requirements, and ps-level response time.

In a recent experiment high intensity infrared (IR) laser pulses directly out of a Ti:Sapphire amplifier were used to illuminate a copper cathode [7]. In this case the electrons are generated through a three-photon process and the current density scales as the third power of the absorbed laser intensity. The experimental results benefitted from the increased IR absorption, up to ∼85%, due to a thin MgF_2 anti-reflective coating. Alternatively, nanoplasmonics concepts could be applied to engineer the optical response of a cathode and obtain high efficiency metallic photocathodes, both through a control of the metal reflectivity and through the effect of the localization of the optical field intensity. This idea was explored by Tsang et al. [8, 9] and more recently by Polyakov et al [10].

Another benefit of a nanostructured cathode is the possibility to control the local charge distribution at the sub-optical-wavelength scale. A recent paper has explored the idea of initializing an electron beam with a nanopatterned charge distribution followed by advanced manipulation schemes for coherent radiation production [11].

In this Letter we report on the first experimental results of the generation of relativistic electron beams from a nanostructured photocathode in a high gradient rf gun. A nanohole array structure was designed and fabricated on a copper surface to obtain a resonant response at ∼800 nm laser wavelength. We measured more than a hundred-fold enhancement in the multiphoton charge yield and report the first characterization of the properties (emittance and bunch length) of such electron beams. The results demonstrated the possibility to manipulate and improve the photoemission performances of a simple material, and mark an encouraging step toward a high efficiency metallic photocathode.

The geometry of the nanostructures consists of a rectangular array of nanoholes fabricated with focused ion beam (FIB) milling on a Cu(100) surface, as shown in Fig. 1(a). The dimensions of the structure, including the spacing p, depth h and FWHM width w of the holes, were optimized through finite-difference-time-

domain (FDTD) numerical simulations [12]. Typical values of h and w are 300 and 200 nm respectively, and p close to 750 nm. When imaging the pattern at normal incidence ($< 1°$) using a narrow bandwidth (2 nm FWHM) laser at the resonant wavelength, the incident light is strongly absorbed, as shown in Fig. 1(c). The measured reflectivity is not sensitive to the aperture of the imaging lens nor small variation of the incident angle, in agreement with FDTD simulation results.

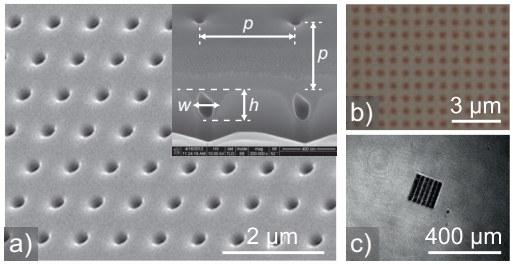

FIG. 1. (Color online) (a) SEM images of the nanohole array. Inset: zoomed-in cut view of the nanoholes. (b) Nanohole array under an optical microscopy with off-resonance visible light. (c) A nanopattern consisting of 6-by-6 25 μm square patches illuminated at resonant laser wavelength.

For our structures, the resonant wavelength mainly depends on the hole spacing and is much less sensitive to the size or even the shape of the nanoholes. Another advantage of this regime is that the aspect ratio of the features is close to unity easing the nanofabrication. The nanohole has an approximately Gaussian profile (Fig. 1(a) inset), mainly due to the current density distribution of the milling ion beam. If the shape of the nanohole is modified to be a square, maintaining the same depth and FWHM width, the resonant wavelength only shifts 4 nm as predicted by FDTD simulation, as shown in Fig. 2(a). This is an important finding that allows us to fine tune the resonant wavelength just by changing the hole spacing p, which is the most accurate and controllable parameter in a FIB machine. As an experimental benchmark, we show in Fig. 2(b) that by decreasing the spacing p from 745 to 710 nm the resonance wavelength shifted from 840 to 813 nm, in good agreement with the simulation prediction. Polarization dependence of the reflectivity at normal incidence was not observed in experiment due to the symmetry of the nanopattern in agreement with simulations.

The bandwidth of the SP resonance is also a critical feature since it is important to match the resonance width with the bandwidth of the photocathode driver laser (∼20 nm). Comparison between the measurement and simulation results in Fig. 2 shows that the resonance of the actual patterns are wider and shallower than what is predicted by simulations. The discrepancy may come from the roughness and residual defects of the copper surface and the stability of the milling ion beams, which in-

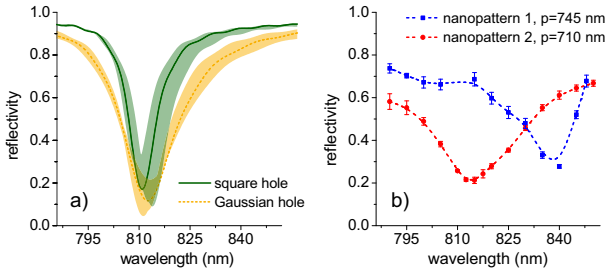

FIG. 2. (Color online) (a) Simulated reflectivity at normal incidence of two arrays of Gaussian (solid) and square (dashed) holes with same p, h and w values. The shaded areas show the results of changing h and w by ±5%. (b) Measured reflectivity of two nanopatterns fabricated on single crystal substrates with 2 nm FWHM bandwidth lasers. The two patterns have same hole width and depth and are only different in spacing.

duce non-uniformity in the pattern. This effect broadens the resonant peaks and was not included in the FDTD modelling. Notably wider resonance bandwidth which supports drive lasers with larger bandwidth and shorter pulse durations can be achieved with alternative nanostructures designs, as reported in Ref. [10].

Testing of the nanopatterned cathodes in a high gradient S-band rf gun took place at the UCLA Pegasus Laboratory [7]. The first nanopatterned cathode installed in the gun was fabricated directly on an ordinary cathode made of polycrystalline copper. Due to the larger variations of the nanoholes caused by random grain sizes and orientations of the substrate, the absorption of the 20 nm FWHM bandwidth drive IR laser was 36%. The rf gun was conditioned to the typical operating gradient of 70 MV/m. An initial concern was the possibility of an increased field emission from the nanopattern. However, comparison with the dark current level from a regular cathode shows negligible difference. This can be explained by the relatively small nanopatterned area compared to the total area of the high field surface of the gun body. Moreover, simulation shows that the maximum DC field enhancement is only 12% due to the lack of sharp edges in the nanopattern.

The effectiveness of the nanopattern to enhance the photoemission is clearly seen in the charge yield map (Fig. 3(a)). IR laser pulses (150 fs FWHM) were focused to 120 μm rms and scanned around the nanopattern at normal incidence ($< 1°$) with a piezo-controlled mirror. The position of the laser spot on the cathode was monitored by a virtual cathode screen, and the beam charge was measured by a calibrated high efficiency beam profile camera. The maximum signal, obtained when the laser spot fully covered the nanopattern, is $Y_{exp} > 1.2 \times 10^2$ times larger than when laser was only hitting the flat surface. The transition between the signal maximum and flat surface is due to the partial illumination of the nanopattern. Interestingly, this large increase can not be

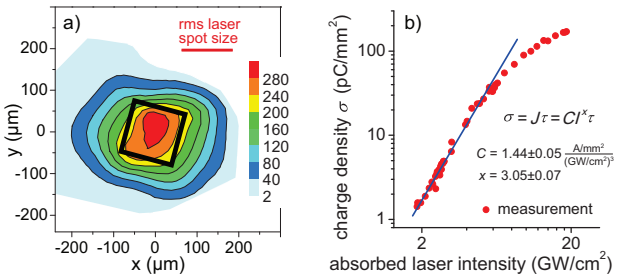

FIG. 3. (Color online) (a) Charge yield map of the nanopatterned cathode. The black square indicates the nanopatterned area. The rms laser spot size is illustrated. (b) The charge density σ versus the absorbed laser intensity. σ is obtained by averaging the measured beam charge over the full pattern area. σ can be expressed as $\sigma = J\tau$ where we choose τ to be equal to the pulse duration of the drive IR laser of 150 fs FWHM and J is an equivalent current density. Fitting of the low charge density part yields a slope of 3.05 ± 0.07.

fully explained by the change in IR absorption. Generalized Fowler-Dubridge theory [13] predicts only an increase of $Y_{FD} = \frac{(1-R_p)^3}{(1-R_f)^3} = 27$ times, where $R_p = 64\%$ and $R_f = 88\%$ are the reflectivity of the nanopattern and the flat surface, respectively.

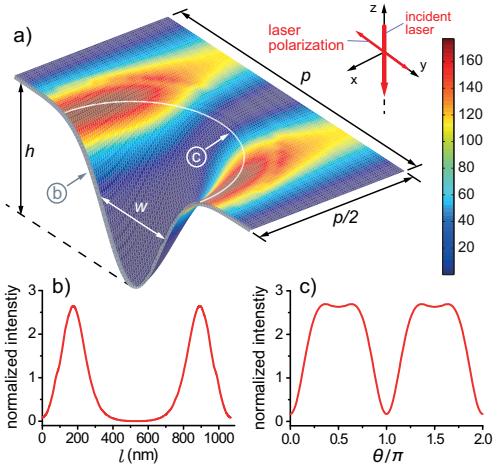

FIG. 4. (Color online) (a) Intensity I distribution on the nanohole surface. The lineouts of I along the metal-vacuum boundaries in the $x = 0$ plane (curve ⓑ, gray line) and $z = -14$ nm plane (curve ⓒ, white line) are shown in (b) and (c) respectively, both normalized by the average intensity over the entire surface.

To understand the additional enhancement in charge emission we look into the details of the optical intensity distribution. In Fig. 4(a) we show the simulated $I \propto |E|^2$ profile at resonant wavelength on the nanohole surface. Two lineouts of the intensity along the metal-vacuum boundary are illustrated in Fig. 4(b) and (c) respectively, both normalized by the average intensity over the entire surface. Due to the third power scaling of the current density versus the laser intensity, concentration of the laser intensity in small local region can significantly enhance the charge yield. We estimate the enhancement factor of the nanostructured surface compared to a flat cathode at equal absorbed intensity by $A = (\int I^3 ds)_{\text{nano}}/(I_f^3 S_f)$, where the integration is performed over the nanohole surface, and S_f and I_f are the area and intensity of the flat surface, respectively. Simulation results predict a factor of $A \leq 14$ for our nanostructure. The experimentally observed enhancement of $A = Y_{exp}/Y_{FD} \sim 5$ is well within the simulation prediction considering the variations of the shapes of the nanostructures.

The increased absorption coupled with the local field enhancement has an important effect also on the damage threshold properties. For the laser pulse durations employed in multiphoton photoemission, typically much shorter than electron-phonon coupling times, the damage threshold is set by the absorbed laser fluence. We measured the damage threshold of the nanopattern. Structural changes were observed when the absorbed fluence approached 10 mJ/cm^2. The result is consistent with that reported on flat copper surface of 50 mJ/cm^2 [14] taking into account the ~ 4.5 times intensity enhancement due to the surface nanopatterning.

It is important to distinguish the multiphoton photoemission regimes from strong optical field emission at nanotips [15–17]. A signature of strong field emitted electrons is a large excess energy spread of a few eV to tens of eV. This is in contrast with the multiphoton regime where the excess energy is typically ≤ 1 eV. The transverse component of the excess energy should be minimized for a low emittance electron source. The Keldysh parameter [18] $\gamma = 73.2\sqrt{\Phi[\text{eV}]/I[\text{GW/cm}^2]}/\lambda[\mu\text{m}]$, where λ is the laser wavelength, Φ is the work function, and I is the laser intensity, is used to evaluate if the emission is in the strong field regime ($\gamma \ll 1$) or the multiphoton regime ($\gamma \gg 1$). For our nanopattern and operating laser intensity γ stays > 10 after taking into account the intensity localization on the surface, deep in the multiphoton regime.

In Fig. 3(b) we show the measured charge density as a function of the absorbed laser intensity under a relatively low extraction field of 25 MV/m. At low intensity the curve has a slope of 3.05 ± 0.07 confirming that the 3-photon process is dominating. Departure from the slope occurs above 40-50 pC/mm^2, similar to that observed on a flat cathode [7], due to the onset of virtual cathode effects [19]. The highest extractable charge density from a cathode is closely related to the maximum achievable beam brightness [20]. Whether the localized emission of photoelectrons from the nanostructured cathode set a different limit on the highest extractable charge density other than a planar cathode case should be an interesting topic for future studies. The results plotted in Fig. 3(b) can be used to estimate that 1.5 μJ, 75 fs FWHM IR drive

laser could generate 30 pC electron beams from a 0.14 mm^2 nanopatterned area assuming full absorption of the drive laser and a high extraction field (> 60 MV/m). In order to generate the same amount of charge with an UV pulse obtained by up-converting the same IR laser pulse, assuming an IR-to-UV conversion efficiency of 10%, it would require a cathode QE of 0.1%, comparable with the most efficient metallic cathodes [21, 22].

The intrinsic emittance of the beam from the nanostructured cathode was measured using the solenoid scan method and the grid (pepper-pot) technique [23]. For these measurements the nanopattern was fabricated on a single crystal copper substrate, which was installed in the gun using a modified cathode back flange. We performed measurements for decreasing (and vanishingly small) beam charges and compared the results with General Particle Tracer (GPT) [24] simulations, as shown in Fig. 5. The observed small increase in emittance versus charge is expected due to the very small initial beam dimensions and thus high charge density at the cathode. Both methods are consistent with an intrinsic emittance value of $\epsilon_{in} = 1.4 \pm 0.1$ mm-mrad per mm rms initial spot size. Values typically reported for ϵ_{in} of a flat copper cathode range from 0.5-1.0 mm-mrad/mm rms [6]. The nanostructured cathode intrinsic emittance can be explained using an initial photoelectron excess kinetic energy comparable to the flat surface case and an additional contribution due to the surface morphology. The curvature of the emission surface increases the initial angles in the electron distribution and distorts the accelerating field lines. We modeled the intrinsic emittance by numerically tracking the photoelectrons using the distorted field lines in the vicinity of each nanohole. With 1.0 eV initial excess energy (corresponding to 0.8 mm-mrad/mm rms) and 35 MV/m launching field the resultant $\epsilon_{in} \approx 1.3$ mm-mrad/mm rms.

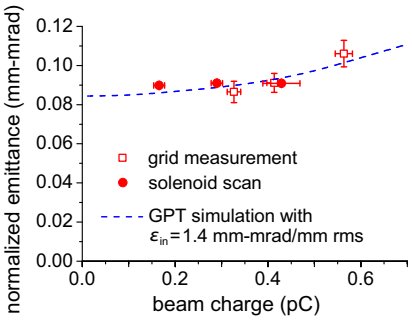

FIG. 5. (Color online) Measurement of intrinsic emittance of the nanostructured cathode using the grid technique (square) and the solenoid scan method (dot), compared with GPT simulation results.

The promptness of the electron emission from the nanostructured cathode was also studied. In SP assisted photoemission, due to the mediation of SPs, the pulse duration of the photoelectrons can depend on the lifetime of the SPs [25]. Based on the width of the resonance curve shown in Fig. 2 we can estimate a relatively low quality factor and thus a damping time comparable to the optical period (3 fs for 800 nm laser). We directly measured the electron beam bunch lengths using the Pegasus X-band rf deflector. We compare the bunch lengths from the nanopatterned area and the flat surface under identical operation conditions. The recorded bunch lengths in the two cases are in good agreement with the GPT simulation assuming prompt emission. The deviations are comparable with the measurement resolution (35 fs) and put an up-limit on the difference of emission time at ∼50 fs. This result supports that the emission from the nanopatterned area has a fast response time.

Finally, regarding the robustness of the nanostructured cathode, we compared its surface morphology before and after the test in the rf photogun. SEM images showed no visible change down to nm scales. This cathode had been exposed to $\sim 10^5$ rf (2 μs long, up to 70 MV/m gradient) and laser (up to 50% of the damage threshold) pulses at a vacuum level of 3×10^{-8} torr. We consider it is reasonable to expect the nanostructured cathode have similar robustness as a ordinary flat copper surface.

In summary, this work demonstrated the possibility of engineering the photoemission properties of a simple cathode material such as a bare copper surface using subwavelength nanostructures to excite properly tuned surface plasmon response. We showed a significant increase in charge yield efficiency and characterized the fast response time, low intrinsic emittance, and robustness of a nanohole array obtained by FIB milling. Experimental results, combined with simulation and theoretical analysis, enabled us to understand the underlying electron emission mechanism, including the effects of optical field localization. We envision that this work can pave a promising step in a new direction of photocathode research. Surface plasmon assisted photoemission could be extended to other metallic and semiconductors surfaces and promise to be an exciting research topic in the generation of high brightness electron beams.

The authors would like to thank Noah Bodzin for his technical support on the fabrication of the nanopattern and Gil Travish for his careful reading and comments of the manuscript. This work was supported by DOE grants DE-FG02-92ER40693, DEFG02-07ER46272, DE-SC0006290, and ONR grant N000140711174.

* musumeci@physics.ucla.edu

[1] W. L. Barnes, A. Dereux, and T. W. Ebbesen, Nature **424**, 824 (2003).
[2] E. Ozbay, Science **311**, 189 (2006).
[3] J. A. Schuller, E. S. Barnard, W. Cai, Y. C. Jun, J. S. White, and M. L. Brongersma, Nature Mater. **9**, 193 (2010).

[4] M. I. Stockman, Phys. Today **64**, 39 (2011).

[5] ICFA Beam Dynamics Newsletter No. 46, edited by M. A. Furman, 2008, http://icfa-usa.jlab.org/archive/newsletter/icfa_bd_nl_46.pdf

[6] D. H. Dowell, I. Bazarov, B. Dunham, K. Harkay, C. Hernandez-Garcia, R. Legg, H. Padmore, T. Rao, J. Smedley, and W. Wan, Nucl. Instrum. Methods Phys. Res., Sect. A **622**, 685 (2010).

[7] P. Musumeci *et al.*, Phys. Rev. Lett. **104**, 084801 (2010).

[8] T. Tsang, T. Srinivasan-Rao, and J. Fischer, Phys. Rev. B **43**, 8870 (1991).

[9] T. Tsang, Opt. Lett. **21**, 245 (1996).

[10] A. Polyakov, S. Cabrini, S. Dhuey, B. Harteneck, P. J. Schuck, and H. A. Padmore, Appl. Phys. Lett. **98**, 203104 (2010).

[11] W. S. Graves, F. X. Kartner, D. E. Moncton, and P. Piot, Phys. Rev. Lett. **108**, 263904 (2012).

[12] FDTD Solutions, http://www.lumerical.com

[13] J. H. Bechtel, W. L. Smith, and N. Bloembergen, Phys. Rev. B **15**, 4557 (1977).

[14] S. E. Kirkwood, A. C. van Popta, Y. Y. Tsui and R. Fedosejevs, Appl. Phys. A **81**, 729 (2005).

[15] M. Schenk, M. Kruger, and P. Hommelhoff, Phys. Rev. Lett. **105**, 257601 (2010).

[16] R. Bormann, M. Gulde, A. Weismann, S. V. Yalunin, and C. Ropers, Phys. Rev. Lett. **105**, 147601 (2010).

[17] H. Yanagisawa, M. Hengsberger, D. Leuenberger, M. Klockner, C. Hafner, T. Greber, and J. Osterwalder, Phys. Rev. Lett. **107**, 087601 (2011).

[18] L. V. Keldysh, Sov. Phys. JETP **20**, 1307 (1965).

[19] D. H. Dowell, S. Joly, A. Loulergue, J. P. de Brion, and G. Haouat, Phys. Plasmas **4**, 3369 (1997).

[20] I. V. Bazarov, B. M. Dunham, and C. K. Sinclair, Phys. Rev. Lett. **102**, 104801 (2009).

[21] H. J. Qian, J. B. Murphy, Y. Shen, C. X. Tang, and X. J. Wang, Appl. Phys. Lett. **97**, 253504 (2010).

[22] J. R. Maldonado, Z. Liu, D. H. Dowell, R. E. Kirby, Y. Sun, P. Pianetta, and F. Pease, Phys. Rev. ST Accel. Beams **11**, 060702 (2008).

[23] R. K. Li, K. G. Roberts, C. M. Scoby, H. To, and P. Musumeci, Phys. Rev. ST Accel. Beams **15**, 090702 (2012).

[24] General Particle Tracer, http://www.pulsar.nl/gpt/

[25] A. Kubo, K. Onda, H. Petek, Z. Sun, Y. S. Jung, and H. K. Kim, Nano Lett. **5**, 1123 (2005).